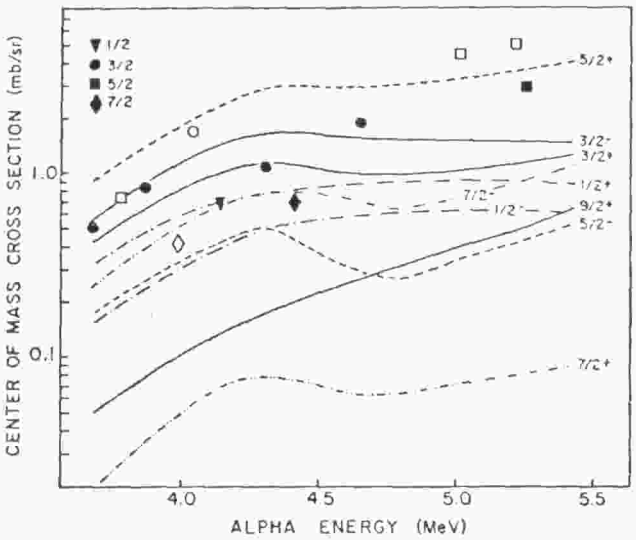

Fig. 5. Normalized theoretical $^{29}Si(\alpha, n_0)^{32}S$ excitation functions and measured on-resonance cross sections at 160° for spin $\frac{1}{2}$, $\frac{3}{2}$, $\frac{5}{2}$ and $\frac{7}{2}$ states in ^{33}S. Solid symbols indicate a pure, single-level resonance is measured whereas open symbols indicate that a secondary state is also contributing.

TABLE 2

Penetrability factors calculated with code MANDYF for the $^{29}Si(\alpha, n_0)^{32}S$ reaction at representative energies, E_α, for specific ^{33}S states, J^π

J^π	E_α (MeV)							
	3.675	3.875	4.135	4.325	4.635	4.920	5.235	5.410
$\frac{1}{2}^-$	0.0281	0.0479	0.0843	0.1158	0.1397	0.1580	0.1693	0.1715
$\frac{1}{2}^+$	0.0612	0.0929	0.1405	0.1739	0.2165	0.2373	0.2410	0.2374
$\frac{3}{2}^-$	0.0278	0.0470	0.0810	0.1086	0.0990	0.1035	0.1087	0.1102
$\frac{3}{2}^+$	0.0212	0.0335	0.0552	0.0714	0.0589	0.0701	0.0796	0.0830
$\frac{5}{2}^-$	0.0042	0.00711	0.0116	0.0153	0.00822	0.0114	0.0171	0.0214
$\frac{5}{2}^+$	0.0231	0.0384	0.0673	0.0924	0.0922	0.1170	0.1378	0.1471
$\frac{7}{2}^-$	0.00416	0.00716	0.0124	0.0170	0.0115	0.0156	0.0227	0.0279
$\frac{7}{2}^+$	0.000313	0.000282	0.000786	0.00106	0.00139	0.00165	0.00204	0.00235
$\frac{9}{2}^-$	0.000006	0.000009	0.000017	0.000041	0.000038	0.000045	0.000072	0.000088
$\frac{9}{2}^+$	0.000752	0.000938	0.000278	0.00324	0.00505	0.000720	0.00949	0.0115
$\frac{11}{2}^{-*}$	0.000010	0.000016	0.000031	0.000060	0.000081	0.000108	0.000195	0.000247
$\frac{11}{2}^+$	0.000000	0.000000	0.000000	0.000000	0.000000	0.000002	0.000002	0.000003

are listed in table 2. On the basis of their dependencies, the cross-section curves reflect a sensitivity to energy and J^π value of the ^{33}S compound nucleus state.

6. Analysis of on-resonance angular distributions

Early in these studies, we established the importance of measuring as full, detailed, and precise an angular distribution as possible on each resonance if a meaningful

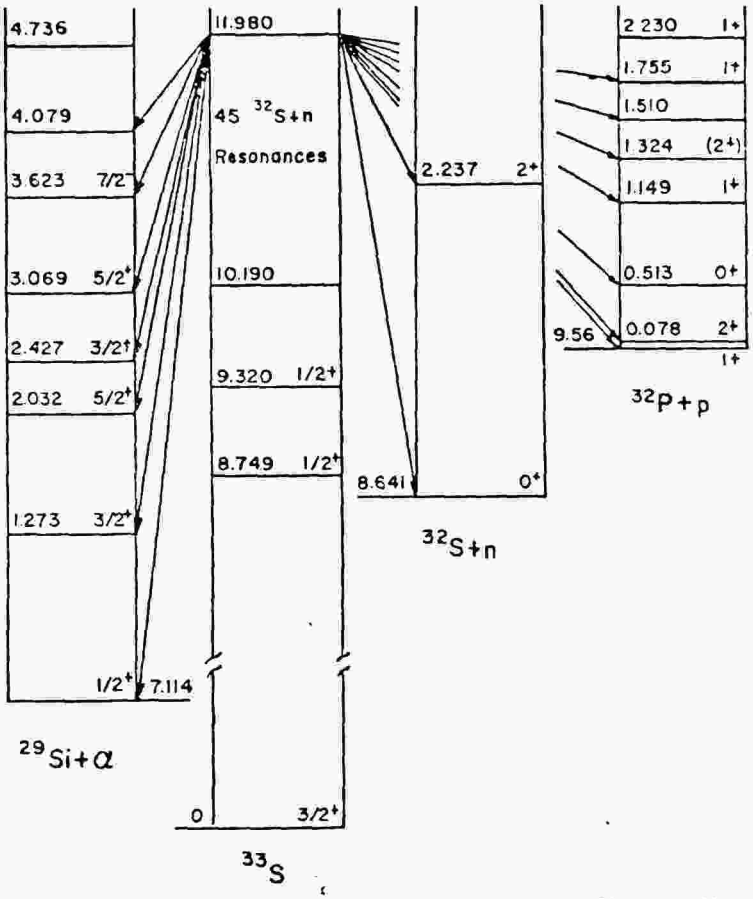

Fig. 6. Energy level diagrams of nuclei in the competing channels for the ^{29}Si(α, n_0)^{32}S cross-section calculation.

analysis was to ensue. To that end on-resonance distributions were measured in 5° steps from 0° to 169°, normalized by the 90° monitor, corrected for neutron background and converted to c.m. absolute cross sections. The targets thickness of ≈ 10 keV provides a compromise between ultimate energy resolution and neutron background effects.

These angular distributions were subjected to both shape and magnitude analysis by code MIA incorporating the same normalization factor of 1.333 established in the single-level analysis. The results of this single- and two-level analysis are shown in figs. 7–11 and the spectroscopic assignments are listed in table 3. The solid curve is the calculated absolute cross section for the specified spin and parity values and the dashed curve is the calculation arbitrarily normalized for shape comparison.

In the analysis, pairs of states up to and including spin $\frac{11}{2}$- and of both parities are mixed coherently. Once the normalization factor of 1.333 was established, the

TABLE 3

Spin and parity assignments for the 42 ^{33}S resonances in the ^{29}Si(α, n$_0$)^{32}S reaction at excitation energies $E^* = 10.344$–11.943 MeV

E_α(lab) (MeV)	E^* (MeV)	Spins and parities	cos δ	R	χ^2_{shape}	Alternative assignments
3.675	10.344	$\frac{3}{2}^{\pm}$		1.19 0.89	7	
3.755	10.411	$\frac{3}{2}^-$, $\frac{5}{2}^-$	−0.27	0.99	3	
3.765	10.423	$\frac{1}{2}^-$, $\frac{5}{2}^-$	0.12	1.45	2	
3.860	10.506	$\frac{3}{2}^{\pm}$		1.64 1.20	8	($\frac{3}{2}^+$, $\frac{5}{2}^+$ cos δ = −0.19, R = 0.60, χ^2 = 10) ($\frac{3}{2}^-$, $\frac{5}{2}^-$ cos δ = −0.15, R = 0.91, χ^2 = 6)
3.875	10.519	$\frac{1}{2}^+$, $\frac{5}{2}^+$	−0.35	0.72	3	
3.945	10.586	$\frac{1}{2}^-$, $\frac{5}{2}^+$	−0.50	0.65	18	
3.985	10.616	$\frac{7}{2}^-$		1.36	40	
4.020	10.647	$\frac{1}{2}^-$, $\frac{3}{2}^+$	−0.12	1.14	6	
4.070	10.691	$\frac{1}{2}^+$, $\frac{5}{2}^-$	0.13	0.80	8	
4.090	10.708	$\frac{1}{2}^-$, $\frac{5}{2}^+$	0.30	0.58	3	
4.135	10.748	$\frac{1}{2}^{\pm}$		0.84 1.30	2	
4.245	10.844	$\frac{1}{2}^-$, $\frac{5}{2}^+$	−0.30	0.53	9	
4.300	10.893	$\frac{3}{2}^{\pm}$		0.85 1.30	4	
4.325	10.915	$\frac{1}{2}^-$, $\frac{5}{2}^+$	−0.30	0.60	47	
4.370	10.954	$\frac{3}{2}^+$, $\frac{5}{2}^-$	0.21	0.55	9	
4.400	10.981	$\frac{7}{2}^-$		1.79	38	
4.425	11.003	$\frac{3}{2}^+$, $\frac{7}{2}^-$	−0.10	0.43	10	
4.440	11.016	$\frac{1}{2}^-$, $\frac{5}{2}^+$	0.15	0.43	2	
4.495	11.064	$\frac{5}{2}^+$, $\frac{5}{2}^+$	−0.38	0.50	6	
4.520	11.086	$\frac{3}{2}^+$, $\frac{5}{2}^+$	0.25	1.85	21	
4.555	11.117	$\frac{1}{2}^+$, $\frac{3}{2}^-$	−0.20	1.68	8	
4.595	11.152	$\frac{7}{2}^-$, $\frac{5}{2}^+$	−0.30	1.26	33	
4.605	11.161	$\frac{1}{2}^-$, $\frac{5}{2}^+$	0.35	1.13	13	
4.635	11.188	$\frac{3}{2}^-$		1.48	8	($\frac{1}{2}^-$, $\frac{3}{2}^-$ cos δ = 0.60, R = 1.76, χ^2 = 5)
4.680	11.227	$\frac{1}{2}^-$, $\frac{3}{2}^+$	−0.35	0.76	8	
4.725	11.266	$\frac{1}{2}^-$, $\frac{1}{2}^+$	−0.50	0.60	6	
4.745	11.284	$\frac{1}{2}^+$, $\frac{7}{2}^-$	0.15	0.49	8	
4.775	11.310	$\frac{5}{2}^+$, $\frac{5}{2}^+$	−0.65	0.54	16	
4.845	11.372	$\frac{3}{2}^-$, $\frac{5}{2}^+$	−0.31	1.50	10	
4.855	11.381	$\frac{1}{2}^+$, $\frac{7}{2}^-$	−0.30	1.60	23	
4.880	11.407	$\frac{1}{2}^-$, $\frac{5}{2}^+$	−0.18	0.61	18	
4.920	11.438	$\frac{3}{2}^-$, $\frac{5}{2}^+$	0.60	0.66	32	
4.970	11.482	$\frac{3}{2}^-$, $\frac{5}{2}^+$	−0.25	0.93	12	
5.100	11.596	$\frac{1}{2}^-$, $\frac{7}{2}^+$	0.27	2.13	3	
5.130	11.620	$\frac{1}{2}^+$, $\frac{5}{2}^+$	−0.80	1.49	49	
5.180	11.666	$\frac{5}{2}^+$, $\frac{7}{2}^-$	−0.30	1.00	6	
5.235	11.714	$\frac{5}{2}^+$		1.07	12	($\frac{5}{2}^+$, $\frac{7}{2}^-$ cos δ = 0.30, R = 0.87, χ^2 = 17) ($\frac{3}{2}^-$, $\frac{5}{2}^+$ cos δ = 0.50, R = 1.31, χ^2 = 11)
5.285	11.758	$\frac{1}{2}^-$, $\frac{3}{2}^+$	−0.20	0.80	33	
5.335	11.802	$\frac{3}{2}^-$, $\frac{5}{2}^+$	−0.20	0.58	46	
5.365	11.829	$\frac{3}{2}^+$, $\frac{5}{2}^+$	0.40	1.57	25	($\frac{5}{2}^-$, $\frac{5}{2}^+$ cos δ = 0.40, R = 1.92, χ^2 = 94)
5.410	11.868	$\frac{1}{2}^+$, $\frac{5}{2}^+$	0.65	1.49	22	
5.495	11.943	$\frac{1}{2}^-$, $\frac{5}{2}^+$	0.05	0.83	12	

The factor, R, multiplies the calculated cross section to provide shape comparison with experimental data. The χ^2_{shape} denotes the χ^2 value in the shape comparison of experimental data to theoretical fits.

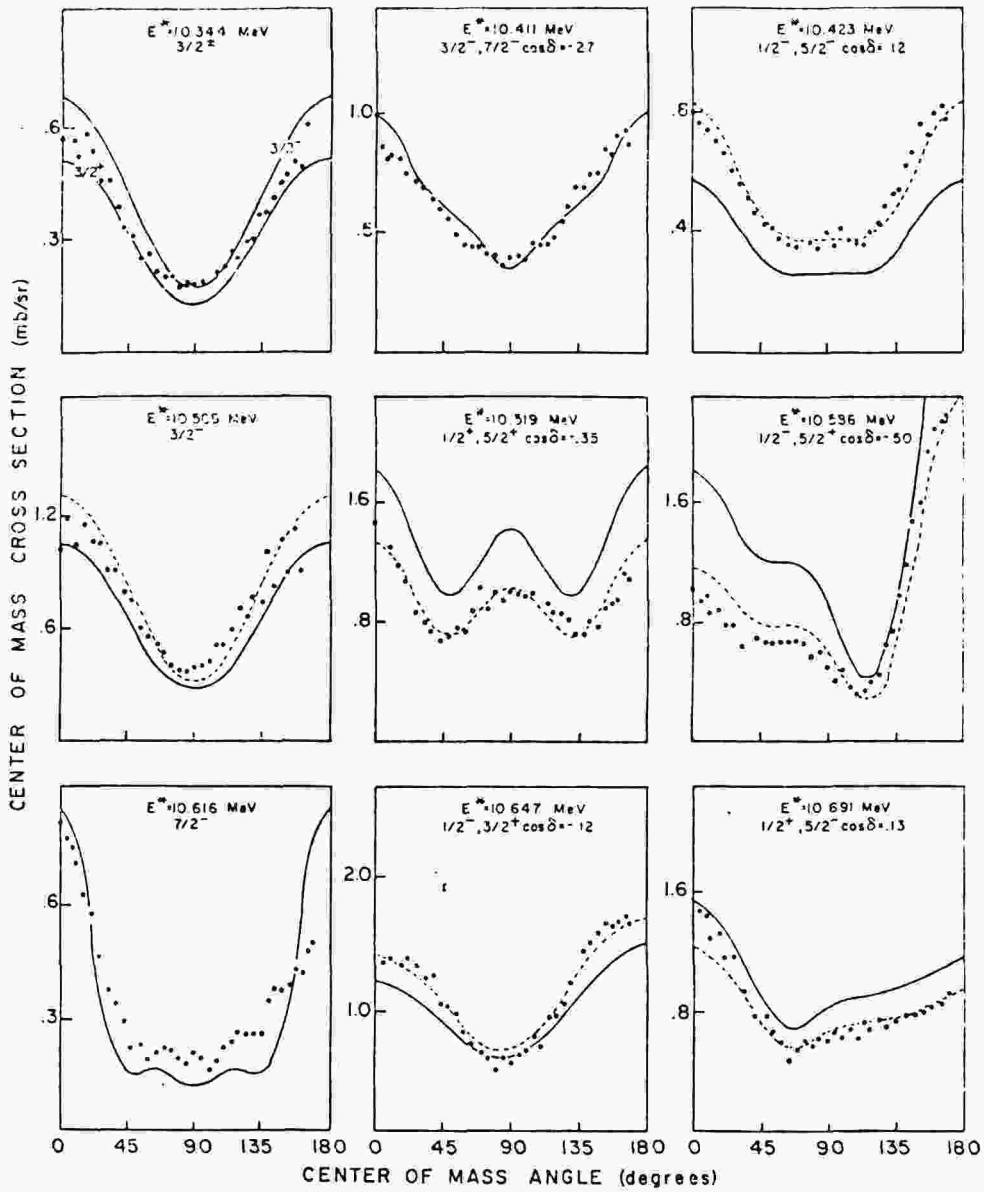

Fig. 7. Comparison of experimental and best-fit theoretical on-resonance angular distributions (solid curves) for the ^{29}Si(α, n$_0$)^{32}S reaction at ^{33}S excitation energies, $E^* = 10.344$–10.691 MeV. The calculated cross sections arbitrarily normalized for shape comparison are plotted as dashed curves.

only free parameter in this process is cos δ, the weighting factor on the interference term. It is automatically cycled from +1.0 to −1.0 in steps of 0.2, subjecting each

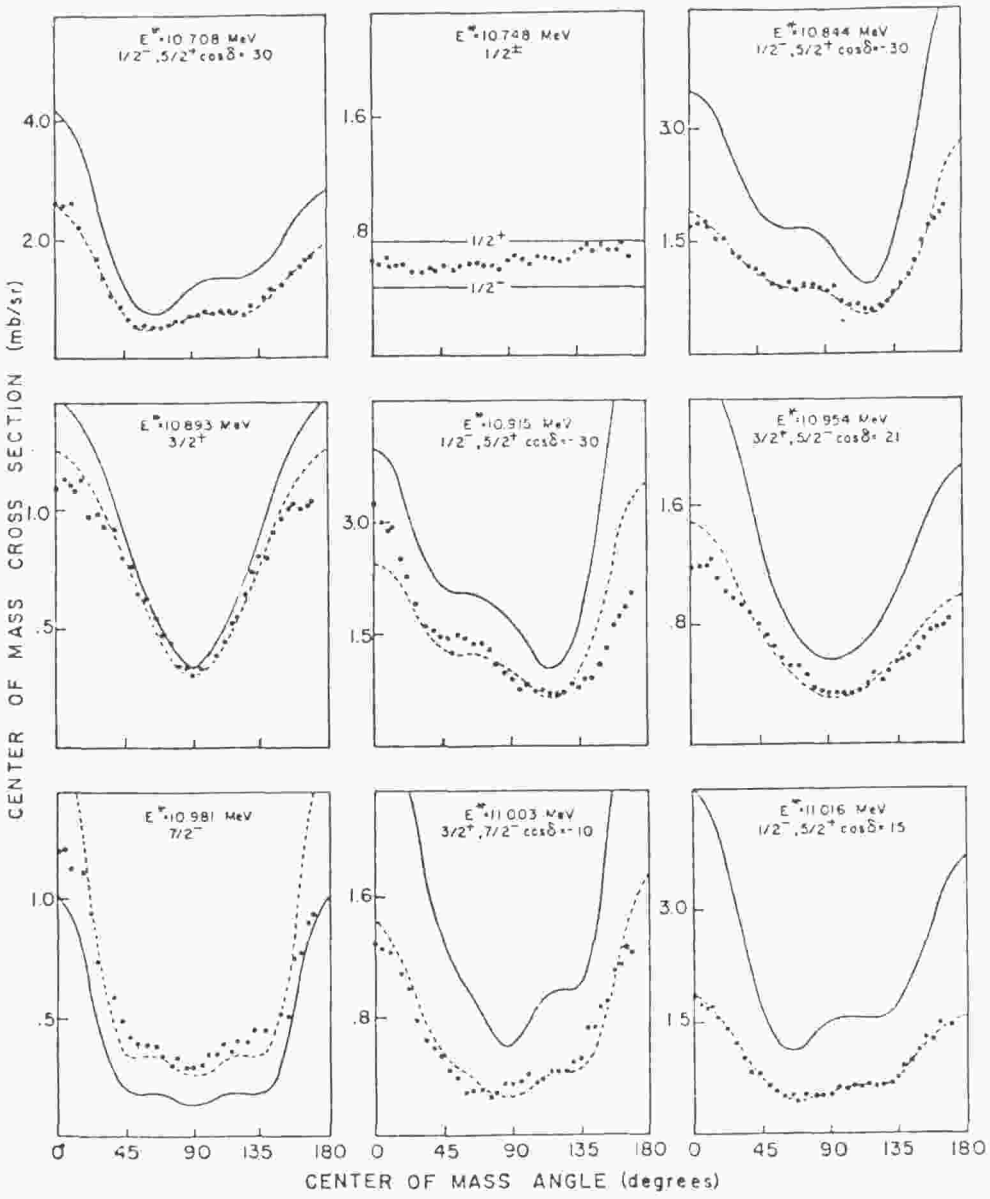

Fig. 8. As fig. 7, but for $E^* = 10.708$-11.016 MeV.

measured distribution to 1452 theoretical fits on the first pass. In the first pass, the vast preponderance of these calculated distributions are automatically rejected on the basis of prespecified χ^2 conditions in shape and (separately) in magnitude. The χ^2 criteria then serve as diagnostic indicators guiding the analysis to the final choice

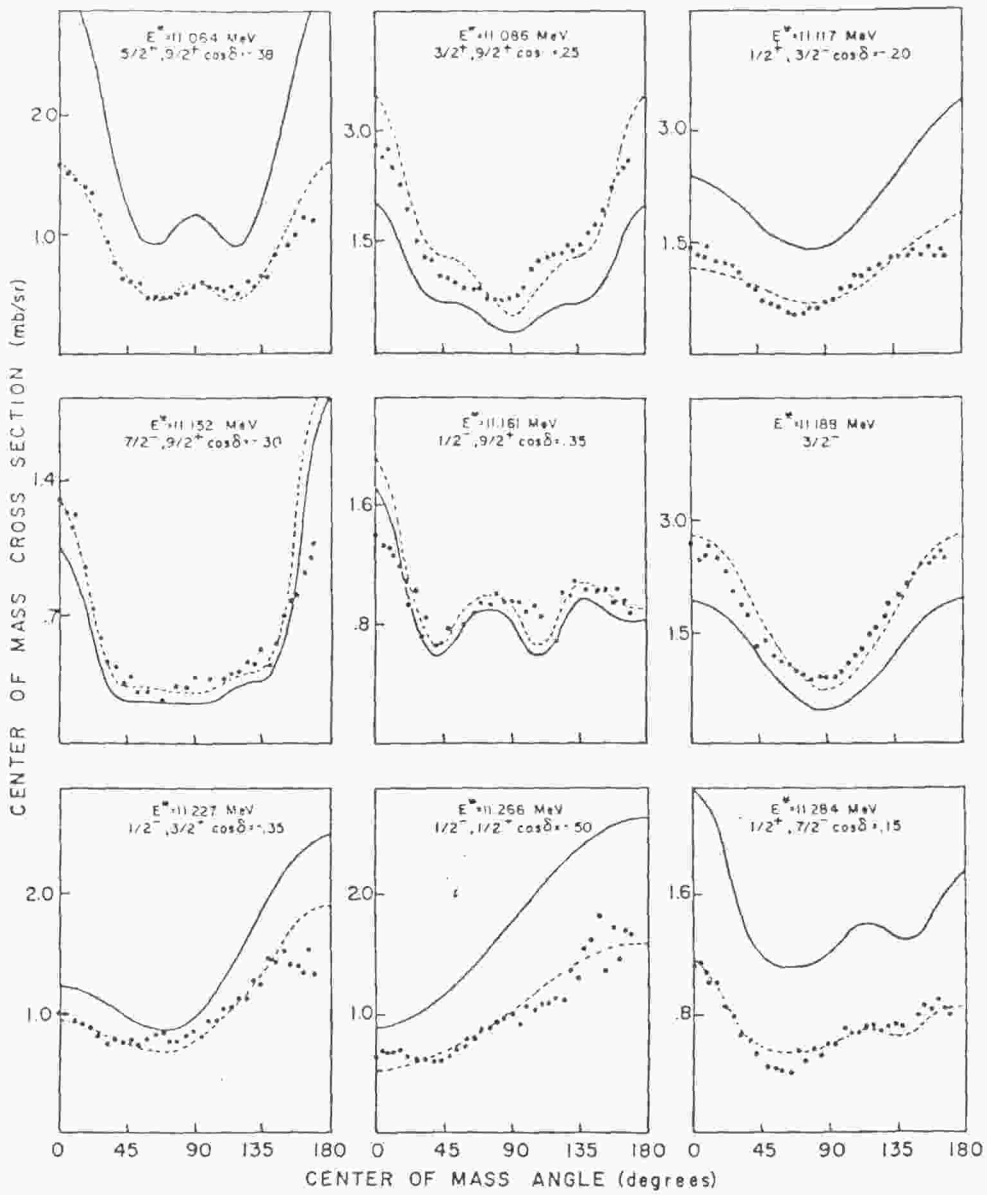

Fig. 9. As fig. 7, but for $E^* = 11.064$–11.284 MeV.

of spin, parity and cos δ values. Table 3 lists the χ^2_{shape} associated with these final choices.

The E^* values are the on-resonance excitation energies in ^{33}S. These energies are corrected for small relativistic effects associated both with the frequency-to-energy

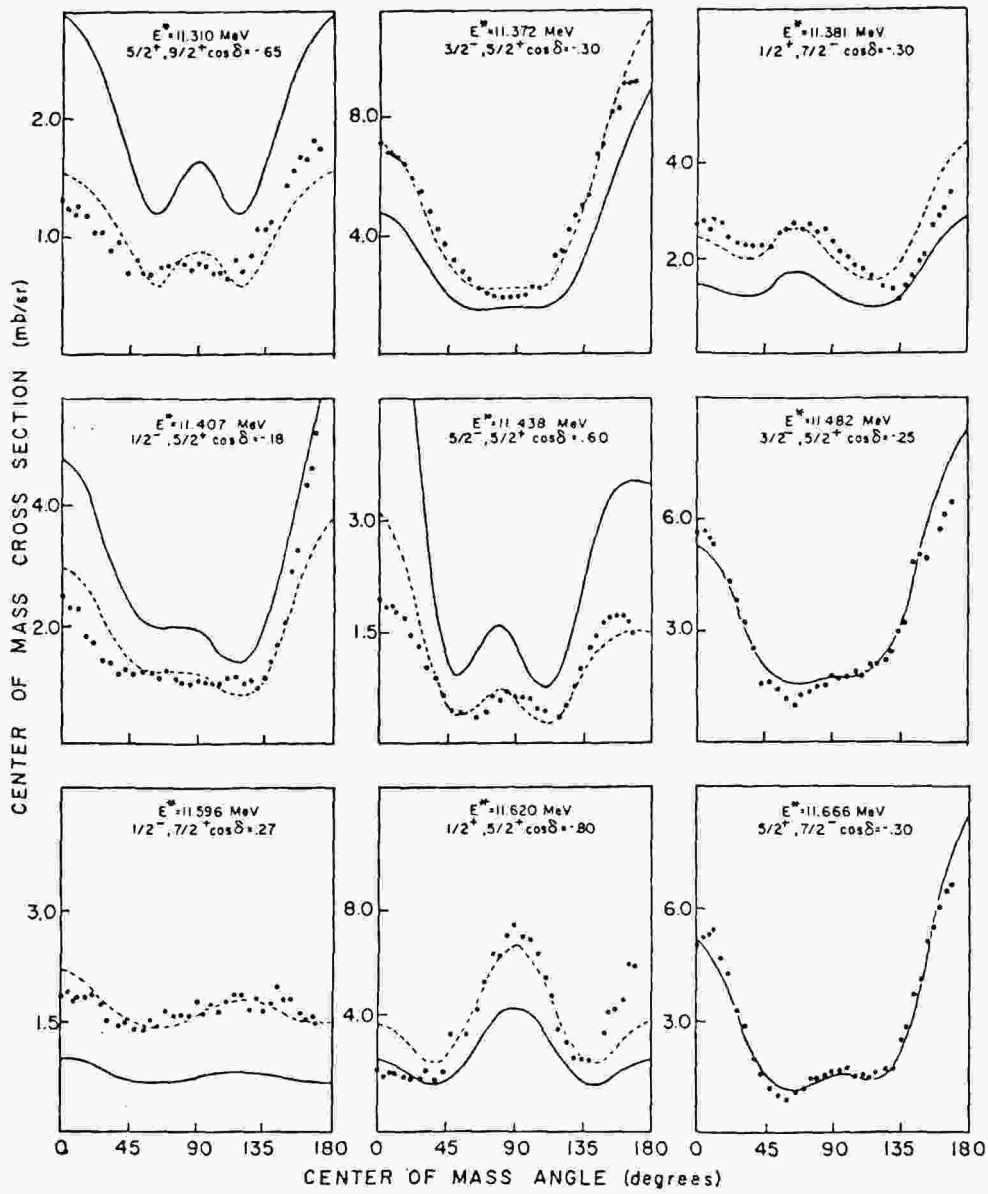

Fig. 10. As fig. 7, but for $E^* = 11.310$–11.666 MeV.

conversion of the beam bending magnetic field and the Q-value equation for $^{29}Si(\alpha, n_0)^{32}S$.

The angular distribution measurements revealed the following interesting features:

(i) Seven resonances were identified as single J^π resonances, with spins of $\frac{1}{2}$, $\frac{3}{2}$, $\frac{5}{2}$ and $\frac{7}{2}$. The remaining 35 resonances were taken to correspond to mixed J^π resonances.

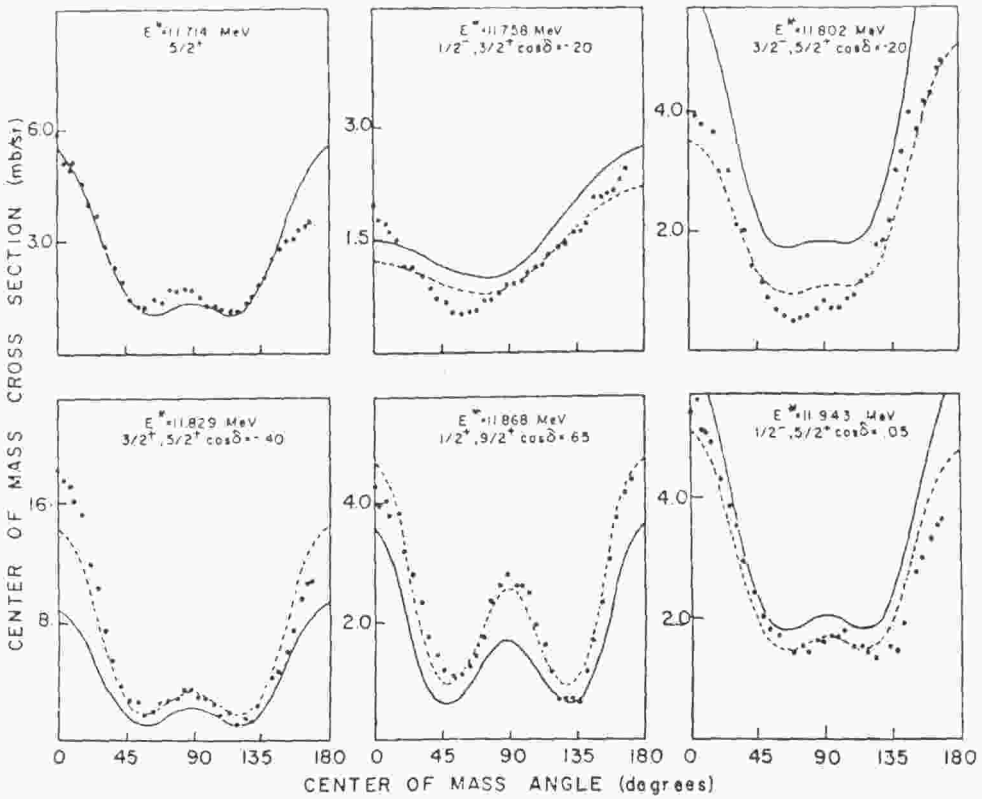

Fig. 11. As fig. 7, but for $E^* = 11.714$–11.943 MeV.

Most of the single J^π resonances occurred at the lower end of the energy range under study, as might be expected from level-density and barrier-penetrability considerations. An additional $\frac{7}{2}^-$ case was discerned at $E^* = 10.616$ MeV but appears to have some admixture due to interferences of at least two other levels; the most likely admixed levels were shown by MIA calculation to be the neighbors $\frac{3}{2}^+$ and $\frac{5}{2}^+$.

(ii) The parity of the spin-$\frac{1}{2}$ case at $E^* = 10.748$ MeV is ambiguous due to the insufficient parity selectivity displayed by the spin-$\frac{1}{2}$ cross sections. The same parity ambiguity is manifested by the spin-$\frac{3}{2}$ assignments at $E^* = 10.344$ MeV and $E^* = 10.506$ MeV. However, in the case of the spin-$\frac{1}{2}$ resonance, the neighbors are both fitted with a $(\frac{1}{2}^-, \frac{5}{2}^+)$ combination, suggesting that the parity of the spin-$\frac{1}{2}$ case is negative.

(iii) As the energy increases, the number of high-spin values also increases, as is predicted by the excitation functions of fig. 6.

(iv) Below $E^* = 11.016$ MeV the predominant spins are $\frac{1}{2}$ and $\frac{3}{2}$ with an uninterrupted sequence of spin-$\frac{1}{2}$ resonances occurring from $E^* = 10.616$ MeV to $E^* = 10.844$ MeV; above $E^* = 11.016$ MeV but below 11.188 MeV, $\frac{9}{2}^+$ admixtures appear

more frequently, while above 11.310 MeV one encounters a region of $\frac{1}{2}^+$ admixtures.

(v) As stated in a previous work [1]) when the parity of two admixing states is the same ($\pi_1 = \pi_2$), the symmetry of the angular distribution about 90° is preserved. Cases in which the parity of the twin levels is the same can be readily observed in resonances at $E^* = 10.411$, 10.423, 10.519, 11.064 and 11.868 MeV. Although they are symmetric, their shape and magnitude do not correspond to that of a pure resonance. On the other hand, when $\pi_1 \neq \pi_2$, the symmetry is in general not preserved, except for the special instance when $\cos\delta = 0$. The parameter $\cos\delta$ governs the amount of disruption of the symmetry about 90° in such a way that for positive values of $\cos\delta$ there occurs a forward peaking in the angular distribution, while for a negative value of this parameter a backward peaking is displayed. A good example of this situation is provided by the results for $E^* = 10.708$ and 10.844 MeV, in which both resonances are fitted with $(\frac{1}{2}^-, \frac{1}{2}^+)$ theory but $\cos\delta$ differs in sign in such a way that they appear to be mirror images of one another.

(vi) The effect that a high negative value of $\cos\delta$ has on the shape of an angular distribution for mixing states of the same parity is shown at $E^* = 11.620$ MeV, fig. 10.

(vii) The importance of having taken into account the largest possible angular range can be shown at $E^* = 11.438$ MeV, where at back angles the angular distribution bends over. This feature made possible an unambiguous assignment of $\frac{5}{2}^-$, $\frac{5}{2}^+$. Other excellent examples of the uniqueness both in shape and magnitude even in the twin overlapping-level case are furnished by the admixtures given in figs. 7–11, especially the resonances at $E^* = 11.266$ MeV and $E^* = 11.868$ MeV.

(viii) In less than 15 % of the entire group of angular distributions investigated did it happen that more than one good fit ensued. Those cases are indicated in table 3 under the column entitled alternative assignments. In the case of the resonance at $E^* = 10.506$ MeV (fitted with spin $\frac{3}{2}$) it is clear that the dominant spin is $\frac{3}{2}$, and that there is some weak interference from either $\frac{7}{2}^-$ or $\frac{5}{2}^+$. The same applies to the $\frac{5}{2}^+$ assignment for the resonance at 11.714 MeV. However, in the case of the resonance at $E^* = 11.188$ MeV an excellent fit was provided by the $(\frac{1}{2}^-, \frac{5}{2}^-)$ admixture, making the present assignment ambiguous. If consideration is taken of the fact that the neighbors of this resonance are admixtures in which the $\frac{1}{2}$-state appears, strong evidence accrues to make the $(\frac{1}{2}^-, \frac{5}{2}^-)$ assignment a very serious competitor. Resonances at $E^* = 11.482$ and 11.829 MeV show clearly that the predominant state J^π in these two cases is a $\frac{5}{2}^+$ state; the complementary J^π state could be either $\frac{3}{2}^-$ or $\frac{7}{2}^-$ for the resonance at 11.482 MeV and either $\frac{3}{2}^+$ or $\frac{5}{2}^-$ for resonance at 11.82 MeV.

(ix) A few of the angular distributions evinced conspicuously poorer fits than the rest (e.g. $E^* = 10.616$, 11.086 and 11.758). This may be suggestive of a three-level involvement in these cases; however a thoroughgoing analysis along these lines was precluded by the resulting ambiguity in spin assignments.